World Journal of Radiology

Online Submissions: http://www.wjgnet.com/esps/
wjr@wjgnet.com
doi:10.4329/wjr.v5.i9.334

World J Radiol 2013 September 28; 5(9): 334-344
ISSN 1949-8470 (online)

ORIGINAL ARTICLE

Impact of field strength and RF excitation on abdominal diffusion-weighted magnetic resonance imaging

Philipp Riffel, Raghuram K Rao, Stefan Haneder, Mathias Meyer, Stefan O Schoenberg, Henrik J Michaely

Philipp Riffel, Raghuram K Rao, Stefan Haneder, Mathias Meyer, Stefan O Schoenberg, Henrik J Michaely, Department of Clinical Radiology and Nuclear Medicine, University Medical Center Mannheim, Medical Faculty Mannheim-Heidelberg University, D-68167 Mannheim, Germany

Raghuram K Rao, the Russel H. Morgan Department of Radiology and Radiologic Science, the Johns Hopkins Hospital, Baltimore, MD 21287, United States

Author contributions: Riffel P, Rao RK and Haneder S performed the majority of the experiments; Rao RK wrote a majority of the manuscript draft; Riffel P organized the data into tables and created figures; Meyer M performed most of the statistical analysis; Schoenberg SO and Michaely HJ oversaw the project from initiation to completion, and helped to edit multiple revisions of the manuscript.

Correspondence to: Dr. Raghuram K Rao, MD, the Russel H. Morgan Department of Radiology and Radiologic Science, the Johns Hopkins Hospital, Musculoskeletal Radiology, 601 N. Caroline Street, Baltimore, MD 21287, United States. rrao2@jhmi.edu
Telephone: +1-443-2876032 Fax: +1-410-2876403

Received: April 30, 2013 Revised: July 17, 2013
Accepted: August 4, 2013
Published online: September 28, 2013

Abstract

AIM: To retrospectively and prospectively compare diffusion-weighted (DW) images in the abdomen in a 1.5T system and 3.0T systems with and without two-channel functionality for B_1 shimming.

METHODS: DW images of the abdomen were obtained on 1.5T and 3.0T (with and without two-channel functionality for B_1 shimming) scanners on 150 patients (retrospective study population) and 10 volunteers (prospective study population). Eight regions were selected for clinical significance or artifact susceptibility (at higher field strengths). Objective grading quantified signal-to-noise ratio (SNR), and subjective evaluation qualified image quality, ghosting artifacts, and diagnostic value. Statistical significance was calculated using χ^2 tests (categorical variables) and independent two-sided *t* tests or Mann-Whitney *U* tests (continuous variables).

RESULTS: The 3.0T using dual-source parallel transmit (dpTX 3.0T) provided the significantly highest SNRs in nearly all regions. In regions susceptible to artifacts at higher field strengths (left lobe of liver, head of pancreas), the SNR was better or similar to the 1.5T system. Subjectively, both dpTX 3.0T and 1.5T systems provided higher image quality, diagnostic value, and less ghosting artifact ($P < 0.01$, most values) compared to the 3.0T system without dual-source parallel transmit (non-dpTX 3.0T).

CONCLUSION: The dpTX 3.0T scanner provided the highest SNR. Its image quality, lack of ghosting, and diagnostic value were equal to or outperformed most currently used systems.

Key words: Abdominal imaging; Diffusion weighted; 3.0T; Radiofrequency excitation; Signal-to-noise ratio

Core tip: With the popularity of 3.0T imaging systems, radiologists have commonly found limitations in abdominal imaging with diffusion-weighted imaging (DWI) secondary to B_1 in homogeneity artifacts at these higher magnet strengths. Because artifacts disturb diagnostic value of abdominal DWI, 1.5T systems have been mainly used for this particular purpose. However, newer techniques involving 3.0T using dual-source parallel radiofrequency (RF) excitation with parallel transmission and independent RF shimming have recently been developed which may succeed in addressing such limitations. Our study illustrates both the objective and subjective utility in the abdominal distribution while imaging under a 3.0T system which incorporates dual-source RF excitation.

Riffel P, Rao RK, Haneder S, Meyer M, Schoenberg SO, Michaely HJ. Impact of field strength and RF excitation on abdominal diffusion-weighted MR imaging. *World J Radiol* 2013; 5(9): 334-344 Available from: URL: http://www.wjgnet.com/1949-8470/full/v5/i9/334.htm DOI: http://dx.doi.org/10.4329/wjr.v5.i9.334

INTRODUCTION

Diffusion-weighted imaging (DWI) is rapidly gaining popularity for assessment of intra-abdominal oncologic and non-oncologic pathologies. Once a technique primarily used in neuroradiology, it is now gaining acceptance as a tool to further characterize alterations of random (Brownian) movement (*i.e.*, diffusion) of water molecules within various lesions in the abdomen[1]. In current clinical settings, this evaluation is mainly performed with 1.5T magnetic resonance (MR) systems; and data from most of the recent investigative studies in the literature have defined lesions within the abdomen using this field strength.

To date, diffusion-weighted imaging has been advocated to have numerous utilities in further evaluating several abdominal and pelvic organs. The technique may be useful in determining pathology in the liver (degree of cirrhosis/fibrosis), kidneys (lesion characterization, renal failure, pyelonephritis), pancreas (pancreatitis and pancreatic cancer), bowel (Crohn's disease), and uterus (endometriosis)[2-18]. In a recent meta-analysis, Li *et al*[19] has shown a potential future role for this type of sequence to assess for cancers within the liver. Numerous lesions within the genitourinary organs (kidneys, ureters, bladder, adrenal glands, uterus, ovaries, and prostate), as well as the adrenal glands, may also eventually be evaluated for malignant potential using similar techniques[12,20-23]. Recently, Padhani *et al*[24] and Koh *et al*[25] have alluded to the promising future of DWI as a cancer biomarker in monitoring response to chemotherapeutic agents, in tumor staging, and possibly to aid in antineoplastic clinical drug development.

Although most of these projections have been forecasted from studies using 1.5T MR imaging systems, in the past few years, more hospitals and practices have begun acquiring 3.0T magnets, due to their ability to acquire images faster, with more detail and with a higher signal-to-noise ratio (SNR)[26-29]. While the image quality is improved broadly across most sequences, DWI in 3.0T systems has been limited by artifacts. These deficiencies are caused by abdominal B_1 field inhomogeneities inherent at 3.0T[30]. B_1 field inhomogeneities can be seen on DWI as a standing wave artifact, mainly as decreased signal intensity[31]. When there is imperfect radiofrequency (RF)-excitation in echo-planar imaging (EPI) sequences such as DWI, poor fat-suppression often results in increased ghosting as well as difficulty in delineating true-positive diffusion restriction (from non-suppressed fat). Because of these limitations, clinical care and clinical studies which require DW images of the abdomen have used 3.0T imaging mainly only in the peripheral structures[32], and data regarding the deeper anatomy have mainly been limited to the 1.5T systems.

Newer techniques involving 3.0T using dual-source parallel RF excitation with parallel transmission and independent RF shimming (dpTX 3.0T), have recently been developed by some vendors, with examples of commercially available products including Siemens TrueForm and Phillips TX. The parallel RF excitation aims to reduce the effects of B_1 inhomogeneity seen in early generation 3.0T scanners (non-dpTX 3.0T). Initial studies by Kukuk *et al*[33] and Willinek *et al*[34] have suggested reduced dielectric effects and an improved homogeneity of the B_1 induction field, particularly over the liver, when comparing these dpTX 3.0T scanners with their non-dpTX counterparts.

Currently no significant data exists to evaluate the differences in image quality of DWI sequences between 1.5T and dpTX 3.0T systems. Therefore, our investigation aimed to objectively compare images produced by the 1.5T, non-dpTX 3.0T, and novel 3.0T scanners which implement dual-source parallel RF excitation. Our aim was to make a comparative analysis of images produced by the three scanners in various abdominal regions across a set of *b*-values commonly used clinically. Besides subjectively grading the image quality, degree of artifact, and diagnostic value, we also objectively measured the SNR of DWI at these various MR-scanners.

MATERIALS AND METHODS

Patients

The study contained two separate populations-one comprised of patients and another consisting of a volunteers. The institutional review board waived the requirement of informed patient consent in the retrospective patient population. Information gathered on this subset was performed in compliance with Health Insurance Portability and Accountability Act (HIPAA) guidelines. For the prospective evaluation, the institutional board approved selection of the volunteers, who signed a written consent form prior to MR imaging.

The first population of 150 patients [mean age, 53.5 ± 18.3 years (SD); age range, 9-82 years; 83 men and 67 women] was retrospectively included as the most recent 50 patients scanned in one of three scanners (1.5T *vs* non-dpTX 3.0T *vs* dpTX 3.0T which implements a dual-source RF excitation technique) up to April 2011. All of the patients were randomly selected to each of the scanners based on availability of the systems, not based on body habitus, disease severity, or claustrophobic considerations; most of the patients selected were of middle-European descent, of which most do not tend to be overly obese. The number of patients with ascites overall selected into any of the three systems did not exceed 10%. The only inclusion criterion was limiting the population to studies of the upper abdomen performed with

Table 1 Imaging parameters in the three imaging systems used for the patient population

	1.5T MR	non-dpTX 3.0T MR	dpTX 3.0T MR
TR/TE, ms	5600/75	6000/76	6400/63
Sequence type	EPI-SE	EPI-SE	EPI-SE
FOV, mm × mm	380 × 308	380 × 308	380 × 308
Matrix	192 × 156	192 × 156	192 × 156
Slice thickness, mm	6	5	5
Interslice gap, mm	0	0	0
Spatial resolution, mm^3	2.0 × 2.0 × 6.0	2.0 × 2.0 × 5.0	2.0 × 2.0 × 5.0
Number slices	32	33	35
b-values	50, 400, 800	50, 400, 800	50, 400, 800
Parallel imaging	GRAPPA 2	GRAPPA 2	GRAPPA 2
Acquisition time, min	4:30	5:06	4:46
Respiratory control	Free breathing	Free breathing	Free breathing
Fat suppression	SPAIR	SPAIR	SPAIR
Averages	4	4	3
Bandwidth, Hz/px	1736	1736	1736

MR: Magnetic resonance.

Table 2 Imaging parameters in the three imaging systems used for the volunteer population

	1.5T MR	non-dpTX 3.0TMR	dpTX 3.0TMR
TR/TE, ms	6300/79	6600/80	6000/68
Sequence type		EPI-SE	
FOV, mm × mm		380 × 297	
Matrix		192 × 150	
Slice thickness, mm		6	
Interslice gap, mm		0	
Spatial resolution, mm^3		2.0 × 2.0 × 6.0	
Number slices		35	
b-values		0, 50, 100, 200, 400, 800	
Parallel imaging		GRAPPA 2	
Acquisition time, min	7:02	7:22	6:54
Respiratory control		Free breathing	
Fat suppression		SPAIR	
Averages		4	
Bandwidth, Hz/px		1628	

MR: Magnetic resonance.

routine protocol diffusion-weighted sequences as laid out below. No exclusion criteria were identified.

The second population of 10 volunteers (mean age, 36 ± 12.2 years; age range, 27-57 years; 6 men and 4 women) was prospectively included and assigned to undergo MR imaging in all three of the abovementioned scanners in a random manner at the same day. No inclusion criteria were identified. The only exclusion criteria were restricting the study from anyone less than 18 years of age and those who had contraindications to MR imaging (incompatible metal implants, cochlear implants, or pacemakers). After volunteering, no volunteers were precluded or excluded from the study.

MR imaging

Three MR scanners were used in this study: an 32-receiver channel 1.5T MR system (MAGNETOM Avanto 32 × 76 1.5T; Siemens Healthcare; Erlangen, Germany), a non-dp TX 32-receiver channel 3.0T MR system (MAGNETOM Trio A Tim System 32 × 76 3.0T; Siemens), and dpTX 64-receiver channel 3.0T MR imaging system with TrueForm design (MAGNETOM Skyra; Siemens). TrueForm addesses the aspect of field homogeneity by using the functionality of a 2-channel transmit array for B_1 shimming by providing uniform radiofrequency distribution in all body regions for optimal B_1 field homogeneity. The two-channel functionality uses different amplitude and phase transmission settings optimized for different body regions. Feeding the two ports of the RF body coil with an optimized weighting (*e.g.*, with elliptical polarization), yielding a homogenous B_1 distribution. The functionality of a 2-channel transmit array works with anatomy-specific settings to reduce B_1 inhomogeneities. All MR scanners were equipped with the same gradient systems. All studies were performed with the systems' standard anterior body matrix coils-six coil elements were included on the 1.5T and non-dpTX 3.0T, while 18 were included on the dpTX 3.0T. In addition, all examinations included a posterior spine matrix coil-six elements on the 1.5T and non-dpTX 3.0T, and eight elements on the dpTX 3.0T. In the patient population, the images were obtained with routinely used *b*-values of 0/400/800 s/mm^2. In the volunteer population, *b*-values were 0/50/100/200/400/800 s/mm^2. All series were acquired during free breathing without respiratory triggering. Slice thickness, interslice gap, and spatial resolution remained similar across all three scanners in both the patient and volunteer population (Tables 1 and 2).

The volunteers underwent diffusion weighted imaging in all of the three scanners on the same day with not more than 10 min between each of the exams.

Image analysis

In each examination, the regions of interest (ROI) were selected manually over eight anatomical distributions, regions mostly chosen due to clinical significance: right lobe of the liver, left lobe of the liver, caudate lobe of the liver, head of the pancreas, right kidney, left kidney, spleen, and muscle (left erector spinae muscle). Care was taken to measure only the intended region without contacting structural borders or obvious vasculature within the anatomical segment. The average size of the sample of tissue obtained for measurement was approximately 1.5 cm^2. Using the ROI-enhancement tool of the OsiriX DICOM viewer (OsiriX 3.7.1; The OsiriX Foundation; Geneva, Switzerland), the mean signal intensity within the ROI was graphically and numerically visualized for each of the measured *b*-values (Figure 1). To calculate noise, an approximately 12 cm^2 elliptical area outside the patient's body, void of ghosting artifact was chosen. The standard deviation of the signal intensity within this region was determined to be the background noise within the image. Measurements from mean signal intensity and noise were then divided to determine the SNR. This process was repeated with all 150 of the hospital patients, and with all ten volunteers.

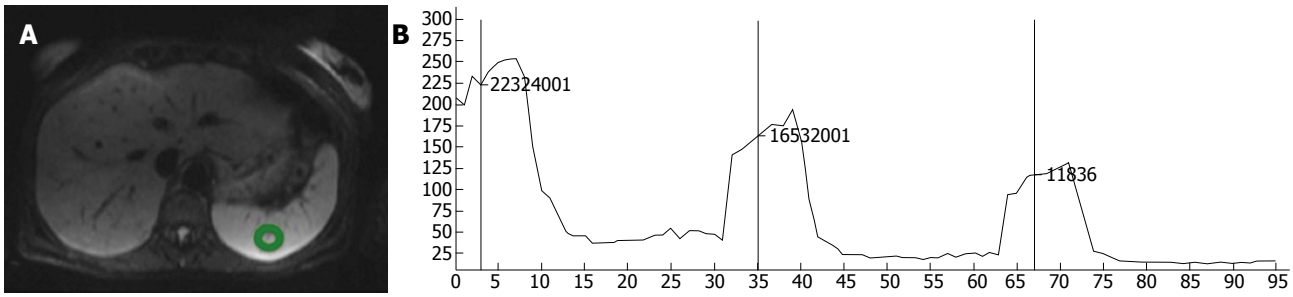

Figure 1 Using the regions of interest-enhancement tool of the OsiriX DICOM viewer for each of the measured *b*-values. A: Representative regions of interest positioned in the spleen; B: With the resultant signal intensities seen for each of the three *b*-values (50, 400, 800).

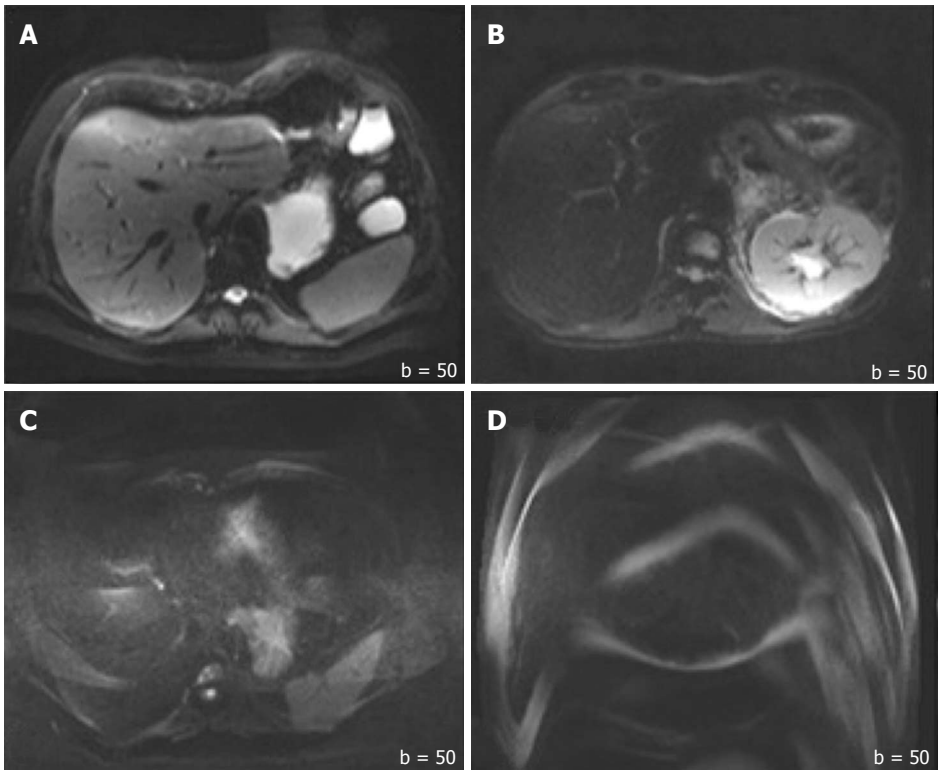

Figure 2 Sample images of quality graded by two radiologists. A: 3 = good for interpretation without noticeable limitations [Image obtained on 2nd gen. 3.0T]; B: 2 = adequate for basic interpretation with minor limitations [Image obtained on 1.5T]; C: 1 = poor for basic interpretation [Image obtained on 1st gen. 3.0T]; and D: 0 = non-diagnostic and not adequate for basic interpretation [Image obtained on 1st gen. 3.0T]. All images were acquired at the same *b*-value (b = 50).

In addition to the SNR, both overall image quality and ghosting artifact were subjectively and independently measured by two radiologists (one with more than 10 years, and another with 1 year of experience in abdominal MR imaging). The overall image quality was scored using an ordinal 4-point rating scale: 3 = good for interpretation without noticeable limitations, 2 = adequate for basic interpretation with minor limitations, 1 = poor for basic interpretation, 0 = non-diagnostic and not adequate for basic interpretation (Figure 2). Ghosting artifacts were scored using a 3-point rating scale: 3 = no ghosting, 2 = ghosting not interfering with diagnostic image interpretation, 1 = severe ghosting artifact interfering with diagnostic interpretation (Figure 3).

The subjective reading results of image quality and ghosting artifacts were used to scale studies for their diagnostic value. This was done by using the more senior radiologist's (Reader 1) ratings (on studies where scoring differed between the two readers). For image quality, images receiving a score of "0" and "1" were combined into a single group called "Non-diagnostic/Low Diagnostic Value," while studies scoring a "2" and "3" were grouped into a single subset identified as "No Loss in Diagnostic Value." This was used to calculate the percentage of studies considered to be diagnostic across each scanner in both populations. Similarly, for ghosting artifacts, a score of "1" was categorized as "Non-diagnostic/Low Diagnostic Value" and scores of "2" and "3" were collectively referred to as "No Loss in Diagnostic Value"; percentages were calculated from each scanner

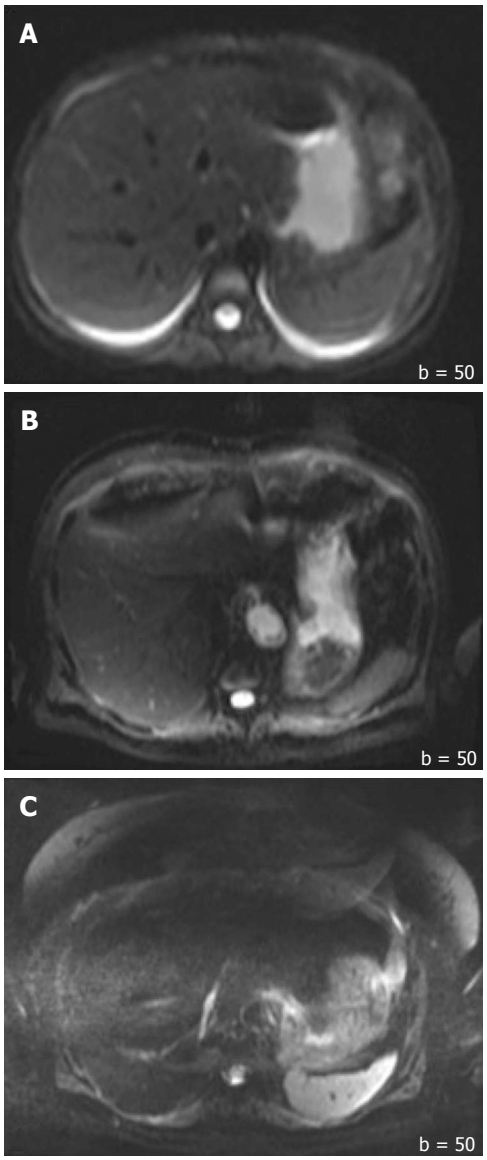

Figure 3 Sample images of ghosting artifact graded by two radiologists. A: 3 = no ghosting; B: Ghosting not interfering with diagnostic image interpretation; and C: 1 = severe ghosting artifact interfering with diagnostic interpretation.

in both populations.

Statistical analysis

Statistical analyses were performed using dedicated statistical software (JMP 9.0, SAS Institute, Cary, North Carolina, United States). The Shapiro-Wilk *W* test was applied to identify normally distributed data. Statistical significance was investigated with a χ^2 test for categorical variables. Differences between groups on continuous variables were assessed using analysis of variance (ANOVA) with post-hoc Scheffé tests to determine group differences. For nonparametric data and for the volunteer population, Kruskal-Wallis ANOVA was used, followed by a post-hoc Mann-Whitney *U* test. Ordinal variables (image quality and ghosting artifacts) were presented as median and were compared using the Kruskal-Wallis ANOVA. Inter-reader agreement was determined by calculating a kappa score. A P value < 0.05 was considered statistically significant.

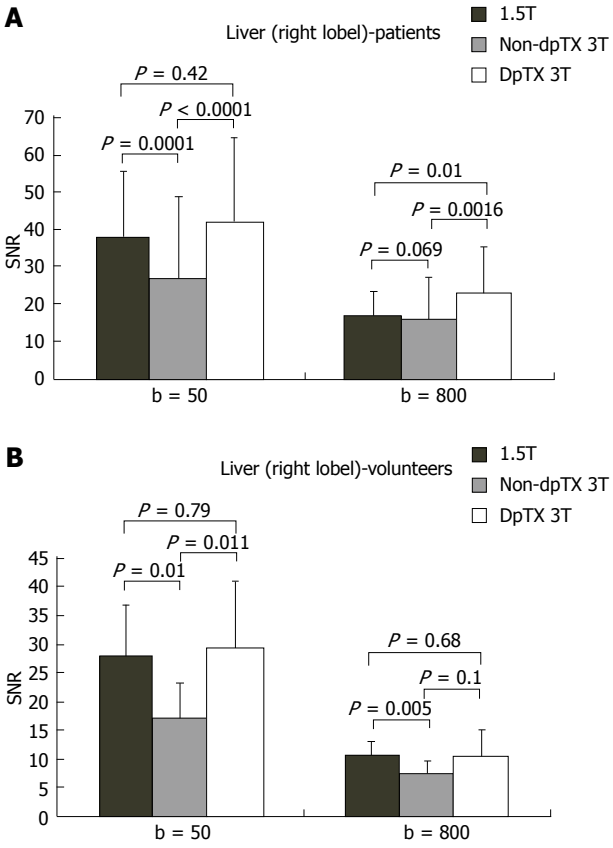

Figure 4 Bar charts of the distribution of signal-to-noise ratio values in the right lobe of the liver at b = 50/800 in the (A) patient and (B) volunteer population. SNR: Single-to noise ratio.

RESULTS

Objective measurements

MR imaging was successfully completed once in all 150 patients and thrice in all 10 volunteer studies. SNR values were calculated in each of the eight anatomical distributions at all the *b*-values for both populations; the collected data is depicted in Table 3.

A total of 14 studies (28%) from the patient population obtained with the non-dpTX 3.0T scanner had such poor image quality and/or artifact (Figures 2D and 3D), that anatomical boundaries (*i.e.*, between lobes of the liver) could not be delineated. These studies were accounted for during the subjective analysis of our investigation. On non-dpTX 3.0T systems, the more peripheral regions (unshaded in Table 3: right lobe of the liver, kidneys, spleen, and muscle) are less susceptible to artifacts. In the patient population, SNR measurements made on the dpTX 3.0T system were higher at the peripheral regions in comparison to the 1.5T and the non-dpTX 3.0T scanners. In the right lobe of the liver (Figure 4A), the dpTX 3.0T captured images of significantly higher SNR when compared to the 1.5T ($P \leq 0.01$ at b = 400/800) and the non-dpTX 3.0T ($P < 0.01$ at all *b*-values). In

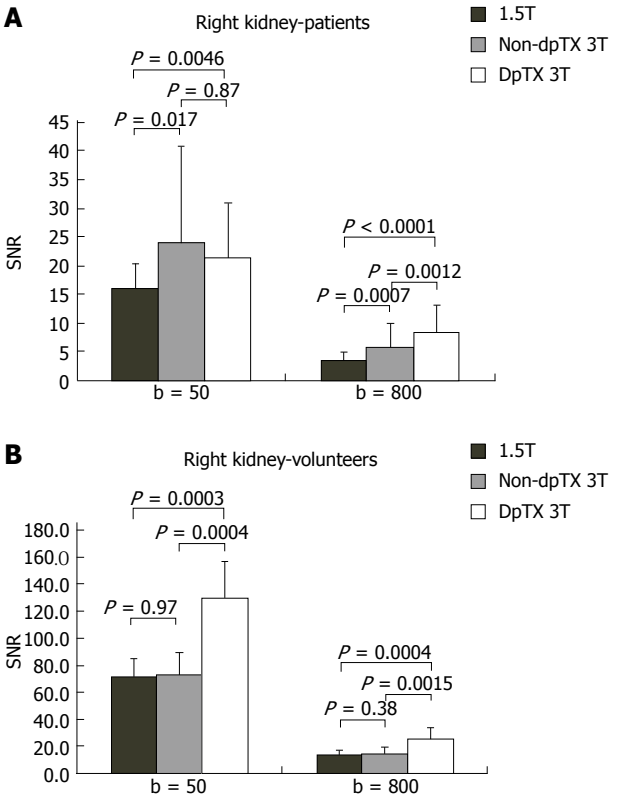

Figure 5 Bar charts of the distribution of signal-to-noise ratio values in the right kidney at b = 50/800 in the (A) patient and (B) volunteer population. SNR: Single-to noise ratio.

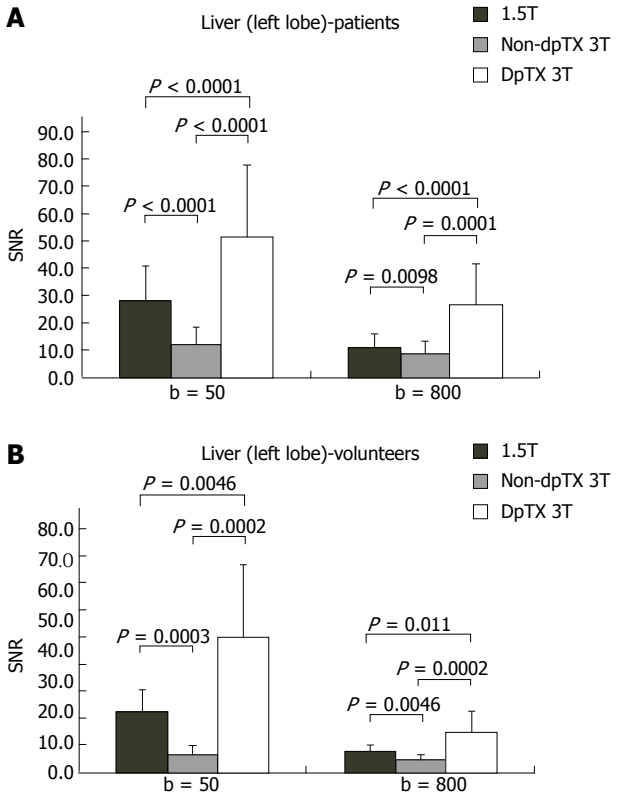

Figure 6 Bar charts of the distribution of signal-to-noise ratio values in the left lobe of the liver at b = 50/800 in the (A) patient and (B) volunteer population. SNR: Single-to noise ratio.

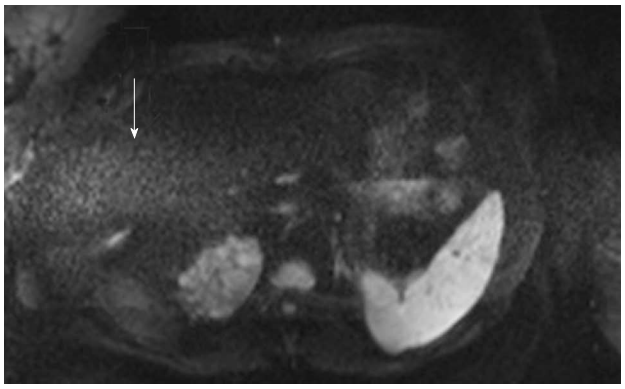

Figure 7 A band of high intensity artifact (arrow) across the middle of the abdomen in diffusion-weighted images obtained on non-dpTX 3.0T (*i.e.*, noise band reconstruction artifact), which contributed to high signal intensity measurements in the caudate lobe and head of the pancreas, as seen on several studies.

this region, the 1.5T scanner displayed a higher SNR than the non-dpTX 3.0T ($P < 0.01$ at b = 50/400). With respect to the kidneys, the 1.5T system produced lower SNR values than both of the 3.0T systems across all the *b*-values ($P < 0.02$ for the right kidney, shown in Figure 5A). Comparing the 3.0T systems, nearly all values from the dpTX scanners were higher than those from the non-dpTX ($P < 0.01$ except at b = 50 in the right kidney). The more central anatomical structures (shaded in Table 3: left lobe of the liver, caudate lobe of the liver, head of the pancreas) are more susceptible to artifacts caused by B_1 inhomogeneity and standing wave artifacts. In the left lobe of the liver, across all *b*-values, the SNR of the dpTX 3.0T systems was highest, followed by SNR values from 1.5T (Figure 6A); all the findings were statistically significant ($P < 0.01$ for all values). In the remaining central regions, the findings were more variable, likely secondary to signal contributions from noise bands due to reconstruction artifacts, which created a band of high signal intensity (Figure 7) and caused an high signal in the non-dpTX 3.0T scanner. The artifact allowed for mean SNR measurements in the caudate lobe to be highest for the non-dpTX 3.0T system at b = 800 ($P \leqslant 0.04$), and although nonsignificant, higher than the 1.5T scanner at b = 400. The dpTX 3.0T scanner showed the highest SNR in the head of the pancreas ($P < 0.01$ compared with the other two scanners at all *b*-values); the non-dpTX 3.0T system produced at least one significantly higher SNR measurement than the 1.5T in this region (at b = 800, $P < 0.01$).

In the volunteer leg of the study, except for similar mean SNR measurements with the 1.5T system in two distributions (the right and caudate lobes of the liver), the mean SNR values from the dpTX 3.0T scanner were significantly higher ($P \leqslant 0.03$ at all values) than the SNR from the other two systems (with two exceptions of non-significant differences: left kidney at b = 400 and spleen at b = 50). As in the patient population, differences of the mean SNR values between the 1.5T and

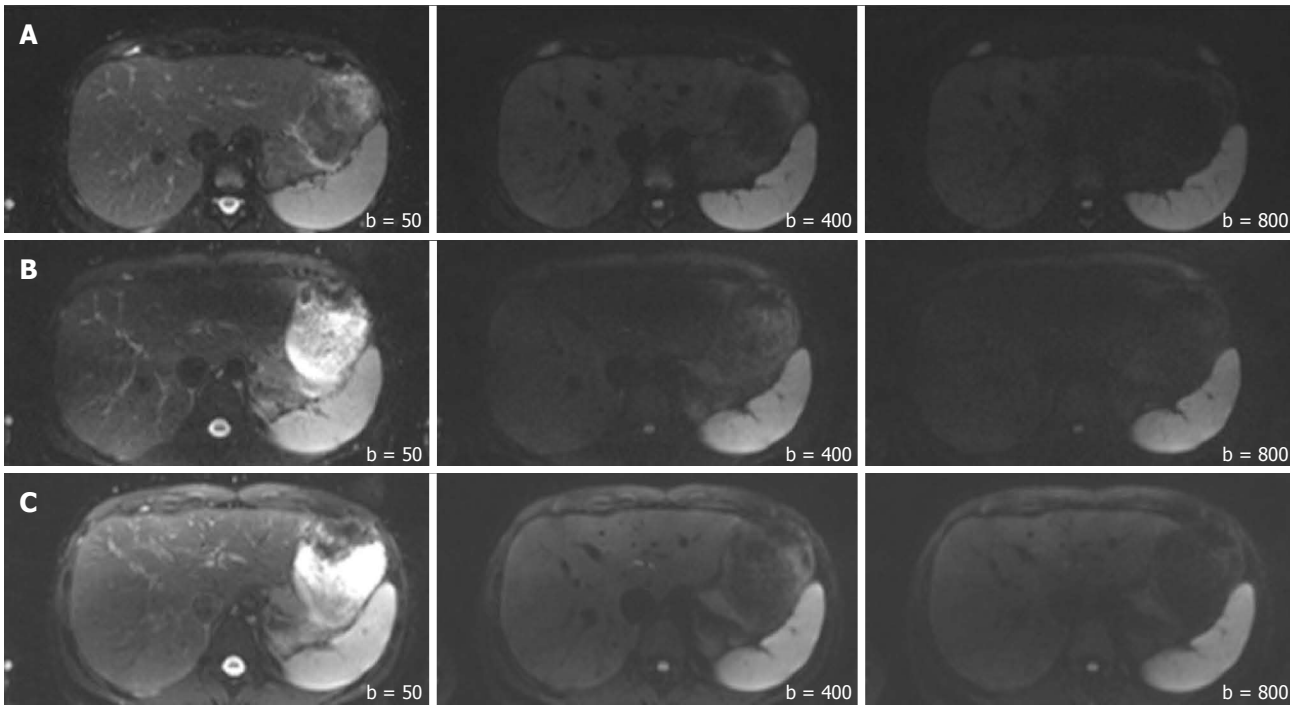

Figure 8 Representative images from the volunteers in the 1.5T (Row A), non-dpTX 3.0T (Row B), and dpTX 3.0T (Row C) scanners. From left to right within each row, *b*-values increase from 50, 400, to 800 s/mm².

non-dpTX 3.0T varied by anatomical region. In the caudate lobe and head of the pancreas, higher signal contributions from band reconstruction artifacts were again responsible for the higher SNR values in the non-dpTX 3.0T system. In the right lobe of the liver, the mean SNR of the 1.5T and dpTX 3.0T systems were similar, with nonsignificant differences at all *b*-values (Figure 4B). Both systems had higher mean SNR measurements than the non-dpTX 3.0T system ($P \leqslant 0.03$ at b = 50/400). The dpTX 3.0T system displayed significantly superior SNR values in nearly all the remaining peripherally-based organs (*e.g.*, right kidney, Figure 5B). The non-dpTX 3.0T system had higher SNR values than the 1.5T scanner in the left kidney ($P \leqslant 0.03$ at b = 400/800), although the differences in the right kidney were not significant. The dpTX 3.0T scanner had significantly higher mean SNR values in centrally-located regions, including the head of the pancreas ($P < 0.01$) and the left lobe of the liver ($P \leqslant 0.01$). In the left lobe of the liver (Figure 6B), the 1.5T system had higher SNR values than the non-dpTX 3.0T ($P < 0.01$).

In summary, when evaluating both the patient and volunteer population, the dpTX 3.0T scanner had the highest SNR at all regions across nearly all the *b*-values, and with a few exceptions, the measurements were statistically significant (Figure 8 and Table 3). The SNR values were usually second-highest in the 1.5T scanner, including central structures such as the caudate lobe and the pancreas (even though reconstruction band artifacts from the non-dpTX 3.0T system caused unnaturally high SNR measurements). The non-dpTX 3.0T generally produced higher values than the 1.5T in the kidneys.

Subjective assessment

When assessing for image quality, both Readers 1 and 2 scored images on the 1.5T and dpTX 3.0T scanners with a median score of "3" in the patient population (Table 4). In the volunteer population, although both readers' median score for the dpTX 3.0T received a "3", for the 1.5T system, Reader 1's median score was 2.5 (*i.e.*, median fell between a "2" and "3"), while Reader 2's score was "3." The non-dpTX 3.0T system received the lowest median score by both readers in both populations, ranging from 1 to 1.5. Table 4 shows that above 94% of the patient and volunteer studies from the dpTX 3.0T and 1.5T scanners were thought to be diagnostic in both the patient and volunteer populations, compared to just 26% of patients and 40% of volunteers in the non-dpTX 3.0T system. Two-sided probability measurements indicates that the differences between the ratings made for the non-dpTX 3.0T scanners and the remaining two systems in both populations were statistically significant ($P \leqslant 0.01$).

As for the ghosting artifacts, in both the dpTX 3.0T and 1.5T scanners, the median scores by both readers was "2" in both the patients and volunteers (Table 5). The median level of ghosting in the patient population with the non-dpTX 3.0T was "1" by both readers, and ranged from 1.5 to 2 in the volunteer population. The measurements indicate that greater 98% of the studies performed on the 1.5T and dpTX 3.0T systems are not hampered by disturbing ghosting artifacts, while only 38% of patients and 80% of volunteers did not reveal disturbing ghosting artifacts with non-dpTX 3.0T systems. Although statistically significant at the patient

Table 3 Mean signal-to-noise ratio measurements for the patient and volunteer populations across all *b*-values in all eight anatomical distributions

		Liver (right lobe)			[1]Liver (left lobe)			[1]Liver (caudate lobe)			[1]Pancreas (head)			Left Kidney			Right Kidney			Spleen			Muscle		
	b-values (s/mm²)	50	400	800	50	400	800	50	400	800	50	400	800	50	400	800	50	400	800	50	400	800	50	400	800
Patients	non-dpTX 3.0T	26.6	19.6	16.3	12.5	9.9	9.1	24.1	18.1	**16.1**	51.6	29.6	21.3	201.7	83.2	(42.4)	168.7[2]	(77.1)	(42.7)	107.8	81.1	59.2	33.2	19.3	11.9
	dpTX 3.0T	42.5[2]	**33.7**	**23.3**	**52.1**	**42.6**	**27.1**	27.3[2]	21.0[2]	12.5	**70.4**	**58.0**	**33.1**	169.0	**138.2**	**65.1**	150.5[2]	**127.6**	**60.0**	118.5	**105.7**	**78.3**	**60.5**	**53.1**	**30.3**
	1.5T	38.1[2]	(24.6)	17.3	(28.6)	(16.8)	(11.3)	24.2	15.2	11.2	40.8	22.6	(14.9)	**118.9**	55.7	28.8	113.3	52.4	26.9	101.9	72.7	52.3	32.1	20.3	(13.4)
Volunteers	non-dpTX 3.0T	17.0	9.4	7.6	6.6	5.3	4.8	**11.6**	6.9	6.3	30.0	14.0	10.2	112.2	44.7[2]	(22.5)	74.0	29.6	16.1	74.7	48.3	33.6	(23.1)	12.3	8.4
	dpTX 3.0T	29.5[2]	14.9[2]	10.7	**44.9**	**20.0**	**13.6**	25.8	11.4[2]	7.9	**76.1**	**30.5**	**18.8**	**155.1**	59.7[2]	**30.8**	**130.5**	**50.4**	**26.3**	106.6[2]	**75.3**	**55.5**	**47.4**	**23.9**	**13.2**
	1.5T	27.9[2]	13.7[2]	10.8[2]	(20.0)	(8.7)	(7.1)	19.0	9.5	7.9	30.1	13.1	9.8	83.4	31.5	16.4	72.2	27.8	14.6	76.3	48.9	34.5	16.6	10.3	8.3

[1]Fields correspond to peripheral anatomical regions, while the [1]fields categorize the central anatomical regions. The numbers which are bolded have statistically higher single-to noise ratio values than both of the other imaging systems at the given *b*-value and regions of interest. The numbers which have a symbol ([2]) have higher Single-to noise ratio (SNR) values than only the lowest SNR measurement at the given *b*-value and region of interest (ROI). Items which are parenthesized are values that have the second-highest SNR, but are still significantly higher than the lowest at the given *b*-value and ROI.

population ($P < 0.01$), the differences were not significant in the volunteer population ($P = 0.47$), due to the low sample size.

For both measurements of image quality and ghosting, the inter-reader agreement revealed a kappa score of 0.8.

DISCUSSION

With the recent increase in popularity of 3.0T imaging systems coupled with the simultaneous boost in applications of abdominal DW imaging, there is a growing interest for data which investigates the validity of using the technologies in combination. Non-dpTX 3.0T scanners, although providing improved image quality/SNR across numerous types of imaging sequences, have had limited applications with DW sequences of the abdomen due to B_1 inhomogeneity artifacts including standing wave and ghosting artifacts experienced in higher field strengths. Improved imaging techniques which incorporate modified radial-like k-Space sampling with fast spin echo DWI (BLADE DWI), have been shown to improve SNR and reduce the level of ghosting and bulk susceptibility artifacts at 3.0T, when compared to standard spin echo echo-planar imaging DWI[35]. However, the findings have been limited to neuroradiological examinations. Because artifacts continue to disturb diagnostic value of abdominal DWI, 1.5T systems have been mainly used for this imaging parameter in both patient care and clinical research. Newer techniques involving 3.0T using dual-source parallel RF excitation with parallel transmission and independent RF shimming, have recently been developed. Feeding the two ports of the transmit array with different amplitudes and a phase shift not equivalent to 90 degrees can potentially result in a more homogeneous B_1 distribution and less signal shading. Recent studies revealed improved image quality in the liver with T2 and DWI sequences when comparing dpTX 3.0T scanners with their non-dpTX counterparts[33,34]. The assessment in these studies was performed subjectively and no controls were used *i.e.*, without volunteers, different patients received examinations.

Our study not only creates controls from volunteers who obtained images from all three scanners, but also introduces a 1.5T imaging system for comparison of image quality. We believe this comparison is essential as 1.5T scanners are considered to have high image quality in DW imaging and are currently the most commonplace field strength utilized to image this sequence. We attempted to present findings in both an objective and subjective method. In our investigation, we could demonstrate that in both patient and volunteer populations, the dpTX 3.0T scanner was characterized by the highest SNR at all measured regions, and across nearly all the *b*-values. In peripherally-located regions, such as the right lobe of the liver and the kidneys, the dpTX 3.0T scanners provided images with significantly superior SNR than the 1.5T and non-dpTX 3.0T systems. The second-best SNR measurements of the right lobe of the liver were produced by the 1.5T scanner, and those of the kidneys, by the non-dpTX 3.0T. Regarding centrally-located regions, the dpTX 3.0T system produced significantly higher SNR values in images in the left lobe of the liver (followed by measurements from the 1.5T scanner) and the pancreas, which is consistent with published data on T2-weighted imaging[34]. The non-dpTX 3.0T system suffered from severe artifacts in these central regions. Evaluation by two radiologists indicated no difference in diagnostic value of the dpTX 3.0T system when compared to 1.5T images. The superior SNR and high level of diagnostic value of the dpTX 3.0T systems are due a reduction of the degree of B_1 inhomogeneity, allowed by a two-way RF transmission, which improves the signal of deeper tissues

Table 4 Image quality: Median values and percent of diagnostic studies

Image quality	Median-Patients		Median-Volunteers		No loss in diagnostic value		Non-diagnostic/low diagnostic value	
	Reader 1	Reader 2	Reader 1	Reader 2	Patients	Volunteers	Patients	Volunteers
non-dpTX 3.0T	1	1	1	1.5	26%	40%	74%	60%
dpTX 3.0T	3	3	3	3	98%	100%	2%	0%
1.5T	3	3	2.5	3	94%	100%	6%	0%

The left half of the table depicts mean values as rated by the two radiologists based on the 4-point ordinal scale in which "3" = good for interpretation without noticeable limitations, "2" = adequate for basic interpretation with minor limitations, "1" = poor for basic interpretation, "0" = non-diagnostic and not adequate for basic interpretation. The right half of the table illustrates the percentage of images deemed to have "No loss in diagnostic value" (scored as $\geqslant 2$) *vs* "Non-diagnositc/Low Diagnostic Value" (scored as $\leqslant 1$). Numbers in bold are statistically different from the other two numbers within the column.

Table 5 Ghosting artifact: Median values and percent of diagnostic studies

Ghosting	Median-Patients		Median-Volunteers		No loss in diagnostic value		Non-diagnostic/low diagnostic value	
	Reader 1	Reader 2	Reader 1	Reader 2	Patients	Volunteers	Patients	Volunteers
non-dpTX 3.0T	1	1	2	1.5	44%	80%	56%	20%
dpTX 3.0T	2	2	2	2	98%	100%	2%	0%
1.5T	2	2	2	2	100%	100%	0%	0%

The left half of the table depicts mean values as rated by the two radiologists based on the 3-point ordinal scale in which "3" = no ghosting, "2" = ghosting not interfering with diagnostic image interpretation, "1" = severe ghosting interfering with diagnostic interpretation. The right half of the table illustrates the percentage of images deemed to have "No loss in diagnostic value" (scored as $\geqslant 2$) *vs* "Non-diagnositc/Low Diagnostic Value" (scored as 1). Numbers in bold are statistically different from the other two numbers within the column.

and reduces artifacts in T2-weighted sequences, such as DWI. Higher SNR can also be accounted for by a multi-element coil ranging, such as the 18-channel body matrix coil in the dpTX 3.0T system, which allow for improved homogeneity of signal; the dpTX 3.0T gradient system is also designed to reduce eddy currents. This implies that with new RF excitation techniques, even artifact-prone sequences such as abdominal EPI sequences can now be acquired with a high success rate.

Non-dpTX 3.0T imaging systems continue to be useful for various other applications within the abdomen, particularly those not affected by B_1 inhomogeneity, such as T1-weighted sequences. T2-weighted imaging, although limited within the abdomen, can be obtained without too much disturbing artifact in certain anatomical distributions (*i.e.*, intracranially). However, only recently has DWI been shown to have sufficient image quality within the abdomen. Our study illustrates both objective and subjective utility of this sequence in the abdominal distribution while imaging under a 3.0T system which incorporates dual-source RF excitation. Because the sampled regions were targeted to investigate clinically-relevant areas and/or distributions where B_1 inhomogeneity is known to cause severe deficiencies with DW imaging in higher field strengths, we believe the findings in our study are important for decisions radiologists will make regarding patient management. To our knowledge, there has been no prior study to show improved SNR or equal diagnostic value of DWI of the abdomen, when comparing 1.5T imaging systems to those of higher field strengths.

Study limitations

The study had limitations. For one, 28% of the studies in the non-dpTX 3.0T patient leg of the study had such significant artifacts, that the data could not be used in calculation of the SNR. The images were, however, used when subjectively rating image quality and diagnostic value. In addition, there are 3 averages used when creating DW images on a dpTX 3.0T, compared to 4 on the other two systems. This additional average would theoretically increase the SNR by $\sqrt{1.3}$, so additional averages by the latter two systems would theoretically cause a higher SNR than the dpTX 3.0T scanner; however despite this disadvantage, the dpTX 3.0T still produced the highest SNR. In the volunteer leg of the study, the number of averages was kept constant for all three scanners. Another limitation is the coils that were used-different body coils and different phased array receiver coils. This likely contributed to differences in SNR, but for the purpose of our investigation, the provided coils were considered part of the system. The patients were selected randomly for each of the scanners; although they were not assigned to scanners based on body habitus, disease type or severity, or claustrophobic conditions, it cannot be fully assured that the images scanned were identical. Therefore a control group was considered by scanning the same volunteers on all three systems. Finally, although the image interpreters were not informed of the types of scans they were evaluating, a true blinding could not be performed as the radiologists, from experience, might have been able to recognize the images as being from one of the three systems. This may have led to bias during subjective grading. The findings of improved SNR and reduced artifact are limited to only those regions imaged within the abdomen.

In conclusion, our findings indicate that dpTX 3.0T scanners which incorporate dual-source parallel RF

excitation with parallel transmission provide diffusion-weighted images of the abdomen with superior SNR, while preserving the image quality and robustness that make 1.5T imaging systems popular. As numerous investigations are currently being performed to assess for pathology/malignancy using diffusion-weighted sequences, it is possible that the improved SNR inherent in newer 3.0T scanners can lead to increased specificity and sensitivity of findings.

COMMENTS

Background

Diffusion-weighted imaging (DWI) is rapidly gaining popularity for assessment of intra-abdominal oncologic and non-oncologic pathologies. In current clinical settings, this evaluation is mainly performed with 1.5T magnetic resonance (MR) systems; and data from most of the recent investigative studies in the literature have defined lesions within the abdomen using this field strength.

Research frontiers

To date, diffusion-weighted imaging has been advocated to have numerous utilities in further evaluating several abdominal and pelvic organs. The technique may be useful in determining pathology in the liver (degree of cirrhosis/fibrosis), kidneys (lesion characterization, renal failure, pyelonephritis), pancreas (pancreatitis and pancreatic cancer), bowel (Crohn's disease), and uterus (endometriosis).

Applications

The dpTX 3.0T scanner provided the highest signal-to-noise ratio (SNR). Its image quality, lack of ghosting, and diagnostic value were equal to or outperformed most currently used systems.

Peer review

The authors compared DW images in the abdomen in 1.5T and 3.0T systems (dpTX 3.0T and non-dpTX 3.0T) in two groups of 150 patients and 10 volunteers. Objective and subjective measures were used to evaluate the indexes of SNR, image quality, ghosting artifacts, and diagnostic value pf DWI among three MR systems. The results showed that the dpTX 3.0T scanner provided the highest SNR with were similar or better performance. The results are interesting.

REFERENCES

1 **Bonekamp S**, Corona-Villalobos CP, Kamel IR. Oncologic applications of diffusion-weighted MRI in the body. *J Magn Reson Imaging* 2012; **35**: 257-279 [PMID: 22271274 DOI: 10.1002/jmri.22786]

2 **Cole DJ**. The reversibility of death. *J Med Ethics* 1992; **18**: 26-30; discussion 31-33 [PMID: 1573646]

3 **Oto A**, Zhu F, Kulkarni K, Karczmar GS, Turner JR, Rubin D. Evaluation of diffusion-weighted MR imaging for detection of bowel inflammation in patients with Crohn's disease. *Acad Radiol* 2009; **16**: 597-603 [PMID: 19282206 DOI: 10.1016/j.acra.2008.11.009]

4 **Shah B**, Anderson SW, Scalera J, Jara H, Soto JA. Quantitative MR imaging: physical principles and sequence design in abdominal imaging. *Radiographics* 2011; **31**: 867-880 [PMID: 21571662 DOI: 10.1148/rg.313105155]

5 **Taouli B**, Koh DM. Diffusion-weighted MR imaging of the liver. *Radiology* 2010; **254**: 47-66 [DOI: 10.1148/radiol.09090021]

6 **Kayhan A**, Oommen J, Dahi F, Oto A. Magnetic resonance enterography in Crohn's disease: Standard and advanced techniques. *World J Radiol* 2010; **2**: 113-121 [PMID: 21160577 DOI: 10.4329/wjr.v2.i4.113]

7 **Manenti G**, Di Roma M, Mancino S, Bartolucci DA, Palmieri G, Mastrangeli R, Miano R, Squillaci E, Simonetti G. Malignant renal neoplasms: correlation between ADC values and cellularity in diffusion weighted magnetic resonance imaging at 3 T. *Radiol Med* 2008; **113**: 199-213 [PMID: 18386122 DOI: 10.1007/s11547-008-0246-9]

8 **Parikh T**, Drew SJ, Lee VS, Wong S, Hecht EM, Babb JS, Taouli B. Focal liver lesion detection and characterization with diffusion-weighted MR imaging: comparison with standard breath-hold T2-weighted imaging. *Radiology* 2008; **246**: 812-822 [PMID: 18223123 DOI: 10.1148/radiol.2463070432]

9 **Galea N**, Cantisani V, Taouli B. Liver lesion detection and characterization: role of diffusion-weighted imaging. *J Magn Reson Imaging* 2013; **37**: 1260-1276 [PMID: 23712841 DOI: 10.1002/jmri.23947]

10 **Lee NK**, Kim S, Kim GH, Kim DU, Seo HI, Kim TU, Kang DH, Jang HJ. Diffusion-weighted imaging of biliopancreatic disorders: correlation with conventional magnetic resonance imaging. *World J Gastroenterol* 2012; **18**: 4102-4117 [PMID: 22919242 DOI: 10.3748/wjg.v18.i31.4102]

11 **Klasen J**, Lanzman RS, Wittsack HJ, Kircheis G, Schek J, Quentin M, Antoch G, Häussinger D, Blondin D. Diffusion-weighted imaging (DWI) of the spleen in patients with liver cirrhosis and portal hypertension. *Magn Reson Imaging* 2013; **31**: 1092-1096 [PMID: 23731536 DOI: 10.1016/j.mri.2013.01.003]

12 **Kim S**, Naik M, Sigmund E, Taouli B. Diffusion-weighted MR imaging of the kidneys and the urinary tract. *Magn Reson Imaging Clin N Am* 2008; **16**: 585-596, vii-viii [PMID: 18926424 DOI: 10.1016/j.mric.2008.07.006]

13 **Yang DM**, Jahng GH, Kim HC, Jin W, Ryu CW, Nam DH, Lee YK, Park SY. The detection and discrimination of malignant and benign focal hepatic lesions: T2 weighted vs diffusion-weighted MRI. *Br J Radiol* 2011; **84**: 319-326 [PMID: 20959371 DOI: 10.1259/bjr/50130643]

14 **Coenegrachts K**. Magnetic resonance imaging of the liver: New imaging strategies for evaluating focal liver lesions. *World J Radiol* 2009; **1**: 72-85 [PMID: 21160723 DOI: 10.4329/wjr.v1.i1.72]

15 **Wang Y**, Chen ZE, Nikolaidis P, McCarthy RJ, Merrick L, Sternick LA, Horowitz JM, Yaghmai V, Miller FH. Diffusion-weighted magnetic resonance imaging of pancreatic adenocarcinomas: association with histopathology and tumor grade. *J Magn Reson Imaging* 2011; **33**: 136-142 [PMID: 21182131 DOI: 10.1002/jmri.22414]

16 **Oto A**, Kayhan A, Williams JT, Fan X, Yun L, Arkani S, Rubin DT. Active Crohn's disease in the small bowel: evaluation by diffusion weighted imaging and quantitative dynamic contrast enhanced MR imaging. *J Magn Reson Imaging* 2011; **33**: 615-624 [PMID: 21563245 DOI: 10.1002/jmri.22435]

17 **Kiryu S**, Dodanuki K, Takao H, Watanabe M, Inoue Y, Takazoe M, Sahara R, Unuma K, Ohtomo K. Free-breathing diffusion-weighted imaging for the assessment of inflammatory activity in Crohn's disease. *J Magn Reson Imaging* 2009; **29**: 880-886 [PMID: 19306416 DOI: 10.1002/jmri.21725]

18 **Kido A**, Fujimoto K, Okada T, Togashi K. Advanced MRI in malignant neoplasms of the uterus. *J Magn Reson Imaging* 2013; **37**: 249-264 [PMID: 23355429 DOI: 10.1002/jmri.23716]

19 **Li Y**, Chen Z, Wang J. Differential diagnosis between malignant and benign hepatic tumors using apparent diffusion coefficient on 1.5-T MR imaging: a meta analysis. *Eur J Radiol* 2012; **81**: 484-490 [PMID: 21333477 DOI: 10.1016/j.ejrad.2010.12.069]

20 **Saremi F**, Knoll AN, Bendavid OJ, Schultze-Haakh H, Narula N, Sarlati F. Characterization of genitourinary lesions with diffusion-weighted imaging. *Radiographics* 2009; **29**: 1295-1317 [PMID: 19755597 DOI: 10.1148/rg.295095003]

21 **Somford DM**, Fütterer JJ, Hambrock T, Barentsz JO. Diffusion and perfusion MR imaging of the prostate. *Magn Reson Imaging Clin N Am* 2008; **16**: 685-695, ix [PMID: 18926431 DOI: 10.1016/j.mric.2008.07.002]

22 **Kilickesmez O**, Inci E, Atilla S, Tasdelen N, Yetimoğlu B, Yencilek F, Gurmen N. Diffusion-weighted imaging of the renal and adrenal lesions. *J Comput Assist Tomogr* 2009; **33**: 828-833 [PMID: 19940645 DOI: 10.1097/RCT.0b013e31819f1b83]

23 **Nishizawa S**, Imai S, Okaneya T, Nakayama T, Kamigaito T, Minagawa T. Diffusion weighted imaging in the detection of upper urinary tract urothelial tumors. *Int Braz J Urol* 2010;

36: 18-28 [PMID: 20202231]
24 **Padhani AR**, Liu G, Koh DM, Chenevert TL, Thoeny HC, Takahara T, Dzik-Jurasz A, Ross BD, Van Cauteren M, Collins D, Hammoud DA, Rustin GJ, Taouli B, Choyke PL. Diffusion-weighted magnetic resonance imaging as a cancer biomarker: consensus and recommendations. *Neoplasia* 2009; 11: 102-125 [PMID: 19186405]
25 **Koh DM**, Blackledge M, Collins DJ, Padhani AR, Wallace T, Wilton B, Taylor NJ, Stirling JJ, Sinha R, Walicke P, Leach MO, Judson I, Nathan P. Reproducibility and changes in the apparent diffusion coefficients of solid tumours treated with combretastatin A4 phosphate and bevacizumab in a two-centre phase I clinical trial. *Eur Radiol* 2009; **19**: 2728-2738 [PMID: 19547986 DOI: 10.1007/s00330-009-1469-4]
26 **Willinek WA**, Schild HH. Clinical advantages of 3.0 T MRI over 1.5T. *Eur J Radiol* 2008; **65**: 2-14 [PMID: 18162354 DOI: 10.1016/j.ejrad.2007.11.006]
27 **Schindera ST**, Merkle EM, Dale BM, Delong DM, Nelson RC. Abdominal magnetic resonance imaging at 3.0 T what is the ultimate gain in signal-to-noise ratio? *Acad Radiol* 2006; **13**: 1236-1243 [PMID: 16979073 DOI: 10.1016/j.acra.2006.06.018]
28 **Heidemann RM**, Griswold MA, Müller M, Breuer F, Blaimer M, Kiefer B, Schmitt M, Jakob PM. [Feasibilities and limitations of high field parallel MRI]. *Radiologe* 2004; **44**: 49-55 [PMID: 14740094 DOI: 10.1007/s00117-003-0977-5]
29 **Schmitt F**, Grosu D, Mohr C, Purdy D, Salem K, Scott KT, Stoeckel B. [3 Tesla MRI: successful results with higher field strengths]. *Radiologe* 2004; **44**: 31-47 [PMID: 14997868]
30 **Schmitz BL**, Aschoff AJ, Hoffmann MH, Grön G. Advantages and pitfalls in 3T MR brain imaging: a pictorial review. *AJNR Am J Neuroradiol* 2005; **26**: 2229-2237 [PMID: 16219827]
31 **Tofts PS**, Barker GJ, Dean TL, Gallagher H, Gregory AP, Clarke RN. A low dielectric constant customized phantom design to measure RF coil nonuniformity. *Magn Reson Imaging* 1997; **15**: 69-75 [PMID: 9084027]
32 **Wang H**, Cheng L, Zhang X, Wang D, Guo A, Gao Y, Ye H. Renal cell carcinoma: diffusion-weighted MR imaging for subtype differentiation at 3.0 T. *Radiology* 2010; **257**: 135-143 [PMID: 20713607 DOI: 10.1148/radiol.10092396]
33 **Kukuk GM**, Gieseke J, Weber S, Hadizadeh DR, Nelles M, Träber F, Schild HH, Willinek WA. Focal liver lesions at 3.0 T: lesion detectability and image quality with T2-weighted imaging by using conventional and dual-source parallel radiofrequency transmission. *Radiology* 2011; **259**: 421-428 [PMID: 21330565 DOI: 10.1148/radiol.11101429]
34 **Willinek WA**, Gieseke J, Kukuk GM, Nelles M, König R, Morakkabati-Spitz N, Träber F, Thomas D, Kuhl CK, Schild HH. Dual-source parallel radiofrequency excitation body MR imaging compared with standard MR imaging at 3.0 T: initial clinical experience. *Radiology* 2010; **256**: 966-975 [PMID: 20720078 DOI: 10.1148/radiol.10092127]
35 **Wintersperger BJ**, Runge VM, Biswas J, Nelson CB, Stemmer A, Simonetta AB, Reiser MF, Naul LG, Schoenberg SO. Brain magnetic resonance imaging at 3 Tesla using BLADE compared with standard rectilinear data sampling. *Invest Radiol* 2006; **41**: 586-592 [PMID: 16772852 DOI: 10.1097/01.rli.0000223742.35655.24]

P- Reviewers Chen F, Wang YX
S- Editor Song XX **L- Editor** A **E- Editor** Liu XM

百世登
Baishideng®

Published by **Baishideng Publishing Group Co., Limited**
Flat C, 23/F., Lucky Plaza,
315-321 Lockhart Road, Wan Chai,
Hong Kong, China
Fax: +852-65557188
Telephone: +852-31779906
E-mail: bpgoffice@wjgnet.com
http://www.wjgnet.com